# Solid-phase partitioning and release-retention mechanisms of copper, lead, zinc and arsenic in soils impacted by artisanal and small-scale gold mining (ASGM) activities

Carlito Baltazar Tabelin [a, *, 1], Marthias Silwamba [b, 1], Florifern C. Paglinawan [c], Alissa Jane S. Mondejar [c], Ho Gia Duc [b], Vannie Joy Resabal [d], Einstine M. Opiso [e], Toshifumi Igarashi [f], Shingo Tomiyama [f], Mayumi Ito [f], Naoki Hiroyoshi [f], Mylah Villacorte-Tabelin [c, g, **]

[a] School of Minerals and Energy Resources Engineering, The University of New South Wales, Sydney, NSW, Australia
[b] Division of Sustainable Resources Engineering, Graduate School of Engineering, Hokkaido University, Sapporo, Japan
[c] Developmental Biology Laboratory, PRISM, Mindanao State University-Iligan Institute of Technology, Iligan City, Philippines
[d] Department of Materials and Resources Engineering and Technology, College of Engineering and Technology, Mindanao State University-Iligan Institute of Technology, Iligan City, Philippines
[e] Geo-environmental Engineering Research Group, Civil Engineering Department, Central Mindanao University, Bukidnon, Philippines
[f] Division of Sustainable Resources Engineering, Faculty of Engineering, Hokkaido University, Sapporo, Japan
[g] Department of Biological Sciences, College of Science and Mathematics, Mindanao State University-Iligan Institute of Technology, Iligan City, Philippines

## HIGHLIGHTS

- ASGM-impacted soils from Davao de Oro, Philippines were evaluated.
- ASGM-impacted soils were highly contaminated with As, Pb and Zn.
- Cu, Pb, Zn and As in the contaminated soil came from sulphide minerals.
- Pb and Zn were strongly retained in the soils via adsorption to HFOs and clays.
- Cu and As release from the historic ASGM site exceeded environmental standards.

## ARTICLE INFO

## ABSTRACT

Artisanal and small-scale gold mining (ASGM) operations are major contributors to the Philippines' annual gold (Au) output (at least 60%). Unfortunately, these ASGM activities lacked adequate tailings management strategies, so contamination of the environment is prevalent. In this study, soil contamination with copper (Cu), lead (Pb), zinc (Zn) and arsenic (As) due to ASGM activities in Nabunturan, Davao de Oro, Philippines was investigated. The results showed that ASGM-impacted soils had Cu, Pb, Zn and As up to 3.6, 83, 73 and 68 times higher than background levels, respectively and were classified as 'extremely' polluted (CD = 30−228; PLI = 5.5−34.8). Minerals typically found in porphyry copper-gold ores like pyrite, chalcopyrite, malachite, galena, sphalerite and goethite were identified by XRD and SEM-EDS analyses. Furthermore, sequential extraction results indicate substantial Cu (up to 90%), Pb (up to 50%), Zn (up to 65%) and As (up to 48%) partitioned with strongly adsorbed, weak acid soluble, reducible and oxidisable fractions, which are considered as 'geochemically mobile' phases in the environment. Although very high Pb and Zn were found in ASGM-impacted soils, they were relatively immobile under oxidising conditions around pH 8.5 because of their retention via adsorption to hydrous ferric oxides (HFOs), montmorillonite and kaolinite. In contrast, Cu and As release from the historic ASGM site samples exceeded the environmental limits for Class A and Class C effluents, which could be

* Corresponding author.
** Corresponding author. Developmental Biology Laboratory, PRISM, Mindanao State University-Iligan Institute of Technology, Iligan City, Philippines.
E-mail addresses: c.tabelin@unsw.edu.au, carlito.tabelin@gmail.com (C.B. Tabelin), mylah.tabelin@g.msuiit.edu.ph, mylahv@gmail.com (M. Villacorte-Tabelin).
[1] These authors contributed equally to this work.

attributed to the removal of calcite and dolomite by weathering. The enhanced desorption of As at around pH 8.5 also likely contributed to its release from these soils.

## 1. Introduction

Gold (Au) is a rare, precious and versatile metal used in various applications ranging from the manufacture of jewellery, electronics (e.g., integrated circuits (ICs) and printed circuit boards (PCBs)), and green, clean and renewable energy technologies to finance and medicine (Calderon et al., 2019, 2020; Jeon et al., 2018a, 2018b, 2019, 2020a, 2020b; Phengsaart et al., 2018, 2020). In 2019, the total global Au demand reached 4368.3 tonnes, 48.5% of which was attributed to jewellery manufacturing while the remainder was in investment (29.2%), technology applications (7.5%), and by Central Banks and other institutions (14.8%) (World Gold Council, 2020a). More recently, Au nanoparticles and nanoclusters are finding unique applications as detectors (Löfås and Johnsson, 1990; Lucarelli et al., 2004), catalysts (Ghenciu, 2002; Zielasek et al., 2006), delivery systems for cancer treatment (Ghosh et al., 2008; Paciotti et al., 2004), and rapid test solutions for viral disease outbreaks like the corona virus disease of 2019 (COVID-19) (Choi, 2020). For the last 5 years, the price of Au in the global market has steadily increased from a low of 1057.4 USD/oz in November 2015 to the current June 2020 value of 1738.2 USD/oz (World Gold Council, 2020b).

The high demand and price of Au, limited economic development in rural areas, and poor implementation of mining laws and frameworks in many developing countries have contributed to the proliferation of artisanal and small-scale gold mining (ASGM), which is estimated to number more than 15 million distinct operations in over 70 countries (Huang and Kilic, 2019; Marshall et al., 2020; Velásquez-López et al., 2011). With the most recent estimates, ASGM activities contribute at least 5% to the annual global production of this precious metal (Hewitt, 2019).

In the Philippines, ASGM operations is an important driver of the economy, accounting for ~63% of Au production from 2005 to 2014 (PSA, 2017). However, the majority of ASGM operations in the Philippines still employ gravity separation-amalgamation—a technique whereby fine and 'free' Au particles are 'pre-concentrated' using gravity separation methods (e.g., sluice boxes and panning) and then recovered by mercury (Hg) (Verbrugge, 2020; Veiga et al., 2014). The resulting Hg–Au amalgam is then heated using retorts or a blow torch to volatilise Hg at ~460 °C and separate it from agglomerated Au particles, yielding a Au doré as final product (Veiga and Hinton, 2002). More recently, ASGM operators in prominent Au mining districts in the Philippines are using a two-step approach to recover more Au from the ores. In the first step, the ores are crushed and Au is recovered via conventional gravity separation-amalgamation while in the second step, tailings from the first step are ground in make-shift ball mills and then fed to an improvised carbon-in-pulp (CIP) circuit (Aseniero et al., 2019; Veiga et al., 2014). The final tailings after CIP are then disposed of in shallow 'pits' close to the processing plant, which readily overflows during the wet season (Opiso et al., 2018).

ASGM activities are one of the primary cause of Hg contamination of the soil in many developing countries. In Mindanao, Philippines, for example, Opiso et al. (2018) reported concentrations of elemental Hg up to ~25 mg/kg in tailings of ASGM operations in four key areas that are, unfortunately, dumped or spread close to the processing areas without treatment. Similar studies of extensive Hg contamination due to ASGM activities have also been reported in Brazil, China, Colombia, Ghana, Ecuador, Indonesia, Mongolia, Peru, Suriname, Tanzania, Venezuela, and Zimbabwe (Babut et al., 2003; Cordy et al., 2011; Male et al., 2013; Mol et al., 2001; Steckling et al., 2011; Swain et al., 2007; Van Straaten, 2000). Another serious environmental problem associated with ASGM activities is soil contamination with hazardous elements like arsenic (As), lead (Pb) and other heavy metals such as copper (Cu) and zinc (Zn), which are typically occluded in sulphide minerals like pyrite ($FeS_2$) found in Au-bearing porphyry ores and hydrothermal deposits (Abraitis et al., 2004; Huston et al., 1995; Nazari et al., 2017; Pirajno, 2009; Tabelin et al., 2012a).

Arsenic is a ubiquitous element in nature notorious for its acute toxicity at high concentrations and chronic toxic effects when ingested at low concentrations for a prolonged and continuous period (e.g., As-contaminated drinking water). Its toxicity is also dependent on the element's oxidation state; that is, arsenite ($As^{III}$) and its oxyanions are more toxic than those of arsenate ($As^V$) (Hughes, 2002). Chronic As poisoning has been shown to increase the risks of developing cancers of the skin, lungs, kidney and liver (Smedley and Kinniburgh, 2002). Similar to As, Pb is a very toxic element and causes serious brain damage and problems with the peripheral system, kidneys and reproductive organs (Needleman, 2004). Meanwhile, Cu and Zn are essential micronutrients for human growth, cardiovascular integrity, normal neuroendocrine and reproductive functions, and healthy iron metabolism and immune system but are toxic at high concentrations (Portnoy et al., 1999; Salgueiro et al., 2000). Dissolved Cu is also harmful to many species of fishes and aquatic invertebrates (Grosell et al., 2007). Unfortunately, very few detailed studies about the extent of soil contamination with As, Pb, Cu and Zn due to ASGM activities have been reported to date.

In this study, soil contamination was investigated in a prominent Au-mining district in Mindanao, Philippines impacted by decades of ASGM activities. Specifically, the objectives of this work are as follows: (1) to identify ASGM-activity derived sources of contaminants, (2) evaluate the extent of soil contamination, (3) to elucidate the release of hazardous elements from the soil using standard leaching tests, and (4) to determine the mechanisms controlling the release from or retention in the soil of hazardous elements under environmentally relevant conditions.

## 2. Materials and methods

### 2.1. Site description and soil sampling procedure

The study area is located in the town of Nabunturan, Davao de Oro (formerly Compostela Valley) about 120 km from Davao City in the island of Mindanao, Philippines (Fig. 1). Davao de Oro is a well-known Au-rich region in the Philippines and has five known porphyry Cu–Au deposits—Kalamatan, Tagpura-Maanob, Amacan, Mapula and Kingking—with Cu and Au grades in the range of 0.34–0.42 wt% and 0.23–0.42 g/t, respectively (Singer et al., 2008). Historically, APEX Corporation operated a large-scale Cu–Au mining operation in the region, but the company went bankrupt in the late 1980s, so Au mining has been dominated by ASGM activities for decades (Verbrugge, 2015).
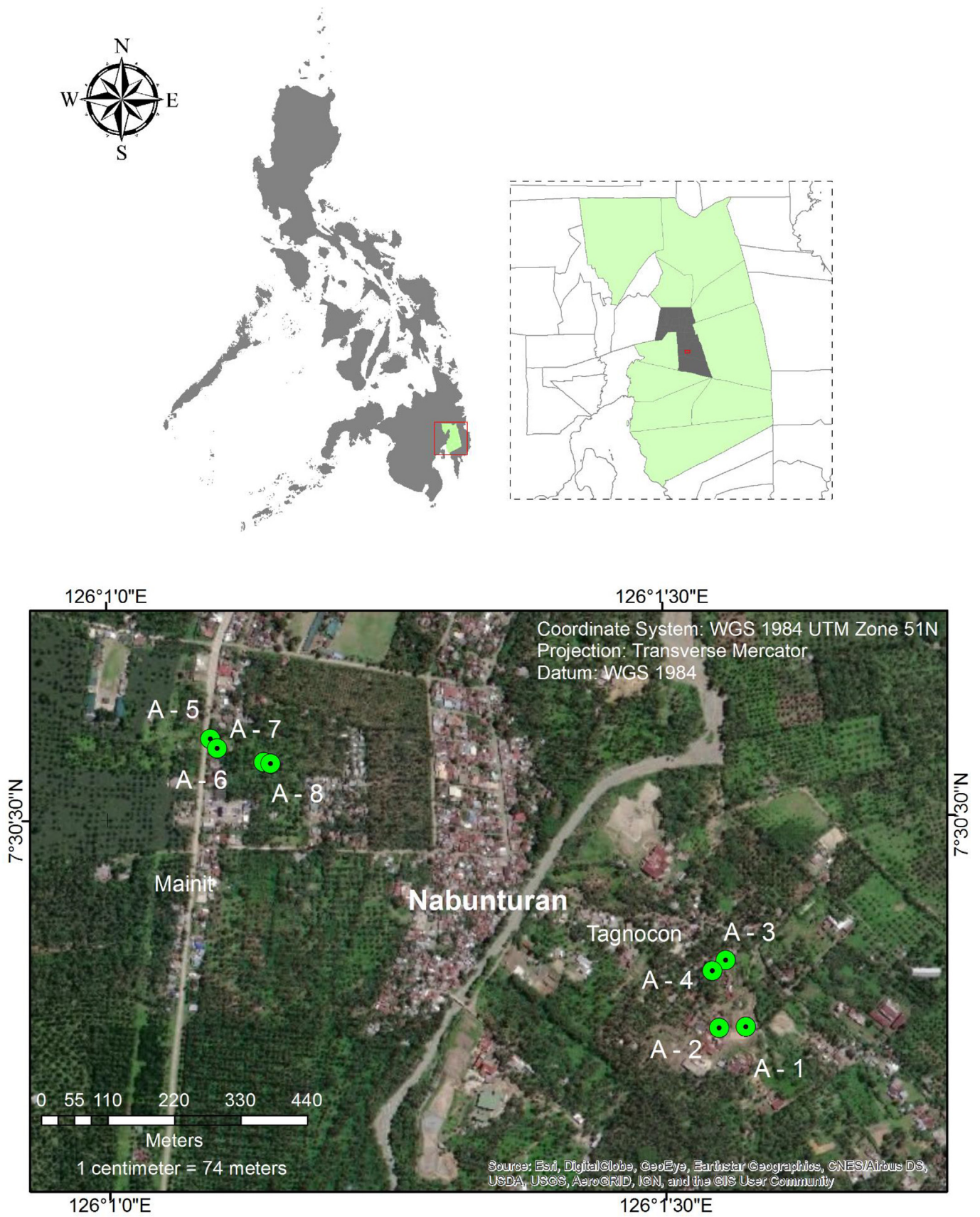
**Fig. 1.** A map of the Philippines superimposed with the sampling locations of ASGM-impacted (A-1 to A-4) and 'control' (A-5 to A-8) soil samples evaluated in this study.

Soil samples were collected from a currently operating site (near the tailings pit (A-1) and Au-ore processing plant (A-2)), a historic processing site (A-3 and A-4) and several uncontaminated (i.e., 'control') areas near the town centre (A-5 and A-6) and a farming area (A-7 and A-8) (Fig. 1). Note that the currently operating site where A-1 and A-2 samples were collected employs the two-step approach of Au-ore processing outlined in the introduction. Using a stainless steel hand shovel, soil samples were collected from a 10 cm by 10 cm area up to a depth of 10 cm and stored in airtight containers. These samples were brought back to the laboratory, air-dried indoors for 7 days and then shipped to Hokkaido University, Japan for characterisation, sequential extraction and leaching experiments.

## 2.2. Characterisation of soil samples and determination of pollution indices

The type of soil was determined by standard particle size analysis using a series of screens (>75 μm) and a laser diffractometer (<75 μm) (L200, Beckman Coulter Inc., USA). For the chemical and mineralogical analyses, the samples were manually ground to <50 μm using an agate mortar and pestle and then analysed by X-ray fluorescence spectroscopy (XRF, NEXCG, Rigaku Corporation, Japan) and X-ray powder diffraction (XRD, MultiFlex, Rigaku Corporation, Japan). XRD peaks were identified using the Match!® software (Crystal Impact, Germany). To measure the total organic carbon (TOC) and inorganic carbon (IC) contents of soil samples, a total carbon analyser equipped with a solid sample combustion unit (TOC-$V_{CSH}$-SSM-5000A, Shimadzu Corporation, Japan) was used. Selected soil samples were also examined by scanning electron microscopy with energy dispersive X-ray spectroscopy (SEM-EDS, InTouchScope™, JSM-IT200, JEOL Ltd., Japan).

Four indices—geo-accumulation index ($I_{geo}$), contamination factor (CF), pollution load index (PLI), and contamination degree (CD)—were determined to evaluate the extent of contamination in the study area due to ASGM activities (Adewumi and Laniyan, 2020). Descriptions and details of how these indices were determined are provided as supplementary information.

## 2.3. Sequential extraction and leaching experiments

Sequential extraction is a widely used technique to identify the solid-phase partitioning of trace contaminants in soils (Tabelin et al., 2014a; Tack and Verloo, 1995), sediments (Huyen et al., 2019a, b; Tack and Verloo, 1995; Tabelin et al., 2012b), rocks (Clevenger, 1990), underground tunnelling wastes (Tamoto et al., 2015), hydrometallurgical residues (Silwamba et al., 2020) and mine tailings (Anju and Banerjee, 2010). In this study, the sequential extraction procedure was based on the earlier works of Marumo et al. (2003), Tessier et al. (1979) and Clevenger (1990). The procedure partitioned the target elements into six environmentally relevant phases or 'functional groups': (1) weakly adsorbed (i.e., water soluble and ion exchangeable), (2) strongly adsorbed (i.e., adsorbed to hydrous ferric oxides (HFOs) and/or phyllosilicate minerals like clays), (3) weak acid soluble (i.e., associated with carbonate minerals), (4) reducible (i.e., occluded in HFOs), (5) oxidisable (i.e., occluded in organic materials and sulphide minerals), and (6) residual (recalcitrant materials).

One gram of sample (<2 mm) and pre-determined volumes of the lixiviants were mixed in 50-mL centrifuge containers using a thermostat water bath shaker. After the pre-determined extraction time, the suspension was centrifuged at 3,500 rpm for 30 minutes to separate the leachate from the residue. The leachate was collected by decantation while the residue was washed with 10−15 mL of deionised (DI) water (18 MΩ cm, Milli-Q® Integral Water Purification System, Merck Millipore, USA) prior to the next extraction step. The leachate and 'washing' solution, which was also collected by centrifugation-decantation, were mixed together, diluted to 50 mL, filtered through 0.45 μm Millex® syringe-driven sterile membrane filters (Merck Millipore, USA) and analysed by inductively coupled plasma atomic emission spectroscopy (ICP-AES, ICPE-9820, Shimadzu Corporation, Japan). The residual fraction was obtained by subtracting the sum of all extracted amounts to that measured by XRF. A summary of the lixiviants and conditions used in each sequential extraction step is listed in Table 1.

The Japanese standard leaching test for contaminated soils (Environmental Agency of Japan Notification No. 46) (JLT-13, 1973; Tabelin et al., 2014b) was used to evaluate the potential release of hazardous elements from ASGM-impacted soils because it closely mimics how pollutants are released when exposed to rainwater. This was done by mixing 15 g of soil sample (<2 mm) and 150 mL of DI water in a 300-mL Erlenmeyer flask at 200 rpm for 6 h. After the leaching experiments, the pH of suspension were measured and the leachate was collected by filtration through 0.45 μm membrane filters. The filtrate was then analysed by ICP-AES for its chemical composition.

Dissolved heavy metals and coexisting ions were quantified using the standard ICP-AES method (margin of error = ±2%). For As concentrations <100 μg/L, the leachate was first pretreated as outlined in our previous work (Tabelin et al., 2013) and analysed by ICP-AES with a hydride-vapour generation system (HVG) (detection limit = 0.1 μg/L; margin of error = ±5%).

## 3. Results and discussion

### 3.1. Changes in soil chemical and mineralogical properties due to ASGM activities

The soil samples collected in the study area were classified as either loamy sand (A-1, A-2, A-3, A-4, A-7 and A-8) or sandy loam (A-5 and A-6) (Supplementary Table 1). The chemical compositions of the soil samples, including their total organic carbon (TOC) and inorganic carbon (IC) contents, are summarised in Table 2. Silica is the main chemical component of all soil samples present mainly as

**Table 1**
Lixiviants and extraction conditions used for the determination of solid-phase partitioning of Fe, Cu, Pb, Zn and As from the ASGM-impacted and 'control' soil samples.

| Step | Extractant | pH | Liquid-to-solid ratio (mL/g) | Temperature (°C) | Duration (h) | Mixing speed (rpm) | Extracted phase |
|------|-----------|-----|------------------------------|------------------|--------------|--------------------|-----------------|
| 1 | 1 M MgCl₂ | 7 | 20/1 | 25 | 1 | 120 | Weakly adsorbed |
| 2 | 1 M NaH₂PO₄ | 5 | 20/1 | 25 | 1 | 120 | Strongly adsorbed |
| 3 | 1 M CH₃COONa | 5 | 20/1 | 25 | 5 | 120 | Weak acid soluble |
| 4 | 0.04 M NH₂OH·HCl in 25% acetic acid | − | 20/1 | 80 | 5 | 120 | Reducible |
| 5 | 0.04 M NH₂OH·HCl in 25% acetic acid; 30% H₂O₂; 0.02 M HNO₃ | − | 36/1 | 80 | 5 | 120 | Oxidisable |
| 6 | Calculated (i.e., Total of each element (XRF) − Sum of each element extracted (Steps 1 to 5) | | | | | | Residual |

*Note: "−" means "not measured".

**Table 2**
Chemical compositions of ASGM-contaminated and 'control' soil samples.

| Sample | SiO$_2$ | Al$_2$O$_3$ | Fe$_2$O$_3$ | MnO | MgO | CaO | Na$_2$O | K$_2$O | TiO$_2$ | S | TOC | IC | Cu | Pb | Zn | As |
|--------|------|------|------|------|------|------|------|------|------|------|------|------|------|------|------|------|
| | (wt%) | (wt%) | (wt%) | (wt%) | (wt%) | (wt%) | (wt%) | (wt%) | (wt%) | (wt%) | (wt%) | (wt%) | (mg/kg) | (mg/kg) | (mg/kg) | (mg/kg) |
| A-1 | 49.2 | 7.36 | 6.83 | 2.88 | 3.24 | 24.6 | 0.0001 | 0.764 | 0.09 | 1.47 | 3.43 | 4.00 | 805 | 6370 | 11,000 | 591 |
| A-2 | 52.8 | 17.3 | 6.05 | 0.70 | 2.27 | 13.5 | 2.96 | 1.57 | 0.35 | 0.31 | 3.44 | 1.71 | 562 | 1960 | 2720 | 121 |
| A-3 | 52.9 | 19.1 | 5.03 | 0.18 | 2.22 | 6.22 | 3.33 | 1.75 | 0.48 | 0.27 | 3.61 | 0.32 | 416 | 1230 | 1220 | 47 |
| A-4 | 51.6 | 21.4 | 6.7 | 0.25 | 2.01 | 5.79 | 2.93 | 2.00 | 0.47 | 0.21 | 5.05 | 0.35 | 380 | 1120 | 1460 | 35 |
| A-5 | 52.8 | 25.5 | 7.63 | 0.08 | 2.54 | 4.03 | 3.64 | 1.88 | 0.72 | 0.07 | 5.20 | 0.10 | 213 | 68 | 235 | 15 |
| A-6 | 50.6 | 25.0 | 7.72 | 0.09 | 2.49 | 5.26 | 3.73 | 1.77 | 0.68 | 0.04 | 5.30 | 0.22 | 218 | 78 | 184 | 15 |
| A-7 | 55.2 | 23.9 | 7.04 | 0.04 | 2.26 | 4.35 | 2.81 | 1.67 | 0.67 | 0.06 | 6.35 | 0.10 | 203 | 74 | 87 | 3 |
| A-8 | 55.1 | 24.8 | 7.45 | 0.08 | 2.26 | 3.08 | 2.69 | 1.62 | 0.73 | 0.06 | 8.03 | 0.03 | 262 | 87 | 97 | 2 |

*Note: Operating ASGM site (A-1 and A-2), historic ASGM site (A-3 and A-4) and 'control' sites (A-5 to A-8).

quartz (SiO$_2$) and anorthite (CaAl$_2$Si$_2$O$_8$), the calcium end-member of plagioclase feldspar (Suplementary Figs. 1 and 2). More prominent calcite (CaCO$_3$) and dolomite ((Mg, Ca)CO$_3$) peaks were detected in A-1 and A-2 compared with the other samples, which could be attributed to the use of locally available limestone by ASGM operators during cyanidation. Supplementary Fig. 2 also illustrates the minor to trace minerals found in soil samples collected from four areas of the site. XRD peaks of pyrite, chalcopyrite (CuFeS$_2$), galena (PbS), sphalerite (ZnS), malachite (Cu$_2$(CO$_3$)(OH)$_2$) and goethite (FeOOH) were detected in A-1 consistent with substantial amounts of Cu (805 mg/kg), Zn (11,000 mg/kg) and Pb (6370 mg/kg) measured by XRF in this sample. Although As-bearing minerals like arsenopyrite (FeAsS) and scorodite (FeAsO$_4 \cdot$2H$_2$O) were not detected by XRD, SEM-EDS observations suggest that As in A-1 was mainly associated with sulphide minerals (Fig. 2; Supplementary Fig. 3) and HFOs (Fig. 3).

Meanwhile, XRD peaks of Clinochlore (Mg$_5$Al(AlSi$_3$O$_{10}$)(OH)$_8$), kaolinite (Al$_2$Si$_2$O$_5$(OH)$_4$) and montmorillonite ((Na, Ca)$_{0.33}$(Al, Mg)$_2$(Si$_4$O$_{10}$)(OH)$_2 \cdot$nH$_2$O) were more prominent in the 'control' samples (A-5 and A-7) than those from the ASGM-impacted sites (A-1 and A-3). Clay minerals in soils are generally formed from the weathering of primary silicate minerals (Balan et al., 2020; Tabelin et al., 2017b; Tabelin et al., 2017c), which means that their lower abundance in ASGM-impacted soils could be attributed to the introduction of unweathered primary silicate minerals (e.g., anorthite) from the tailings. This relationship was also observed in lower Al$_2$O$_3$ contents of A-1 compared with other samples as well as the <50 CWI and PIA values of A-1 classifying it as relatively unweathered (Table 3) (McLennan et al., 1993). This dilution effect was also implied by the less pronounced XRD peaks (i.e., lower abundances) of Clinochlore, kaolinite and montmorillonite in A-1 and A-2 compared with those in A-3 to A-8 (Supplementary Figs. 1 and 2).

### 3.2. Extent of soil contamination due to ASGM activities

Exceptionally high Cu, Pb, Zn and As were found in the soil samples impacted by ASGM activities (Table 2). Using the average values measured in the 'control' samples as baseline, Cu, Pb, Zn and As in the currently operating ASGM site (A-1 and A-2) were 2.5–3.6, 25–83, 18–73 and 13–68 times higher than baseline levels, respectively. In comparison, these four elements were dramatically lower in soils collected from the historic ASGM processing plant (A-3 and A-4) at 1.6–1.8 (Cu), 14–16 (Pb), 8–10 (Zn) and 4–6 (As) times higher than baseline levels. The high heavy metal abundance of the 'control' samples could be attributed to the unique site geology as highlighted previously. In contrast, the average As content of 'control' samples was well within the 1–10 mg/kg values reported for soils formed from igneous and sedimentary rocks (Tabelin et al., 2010; Tabelin et al., 2018).

Table 3 summarises the values of soil pollution indices—$I_{geo}$, CF, CD and PLI—and the results showed 'extreme' pollution with Pb, Zn and As (CD = 30–228; PLI = 5–35) in both currently operating (A-1 and A-2) and historic (A-3 and A-4) ASGM processing sites. Interestingly, the degrees of Cu contamination based on $CF_{Cu}$ in these areas were from 'moderate' to 'considerable' degrees only, which could be attributed to the very high baseline levels of Cu in soils of the study site. Similar interpretations were obtained using the $I_{geo}$ values; that is, A-1 and A-2 were 'heavily' to 'extremely' polluted with Pb, Zn and As while A-3 and A-4 were 'moderately' to 'heavily' contaminated with these three contaminants. Soil contamination in the area was likely exacerbated by two factors: (1) the local miners' practice of intentionally 'spreading' tailings and waste rocks on the processing area, and (2) frequent overflowing of the shallow tailings pit during the rainy season.

### 3.3. Solid-phase partitioning of copper, lead, zinc and arsenic in ASGM-impacted and 'control' soil samples

Copper in A-1 and A-2 (currently operating ASGM processing site) was mainly partitioned with the oxidisable (23–37%), strongly adsorbed (24–31%), weak acid soluble (19–21%) and reducible (12–16%) fractions (Fig. 4). The high amounts of Cu associated with oxidisable and weak acid soluble fractions could be attributed to the presence of chalcopyrite and malachite in these samples while those in the reducible fraction are occluded with HFOs like goethite (Fig. 3). Strong associations of Cu with Fe in HFOs could be attributed to co-precipitation of these metal ions between pH 4 and 9, a phenomenon well-known in ore genesis, hydrometallurgy, and treatment of acid mine drainage (AMD) and municipal/industrial wastewaters (Igarashi et al., 2020; Tomiyama et al., 2019, 2020; Veiga et al., 1991). Igarashi et al. (2020), for example, noted that the removal of Cu$^{2+}$ and Zn$^{2+}$ in AMDs occurred via their co-precipitation with HFOs rather than as distinct and separate Cu- and Zn-oxide minerals. Similarly, the bulk of Cu in the strongly adsorbed fraction was most probably associated with HFOs like goethite, which are well-known for their strong heavy metal sorption capacities above around pH 7.5 (Park et al., 2019; Tabelin et al., 2014c; Tatsuhara et al., 2012; Violante et al., 2003; Veiga et al., 1991). According to Hua et al. (2012), adsorbed Cu$^{2+}$ on goethite are not readily mobilised because it forms inner sphere complexes that have intrinsic adsorption rate constant about two orders of magnitude higher than the intrinsic desorption rate constant.

Similar to A-1 and A-2, Cu in A-3 and A-4 was mainly partitioned with the four phases discussed previously. Two noteworthy differences, however, are the lower Cu found in oxidisable fraction of soil samples from the historic ASGM processing site (A-3 and A-4) and the higher Cu associated with weak acid soluble phase (Fig. 4a and b). These differences could be explained by longer exposure of
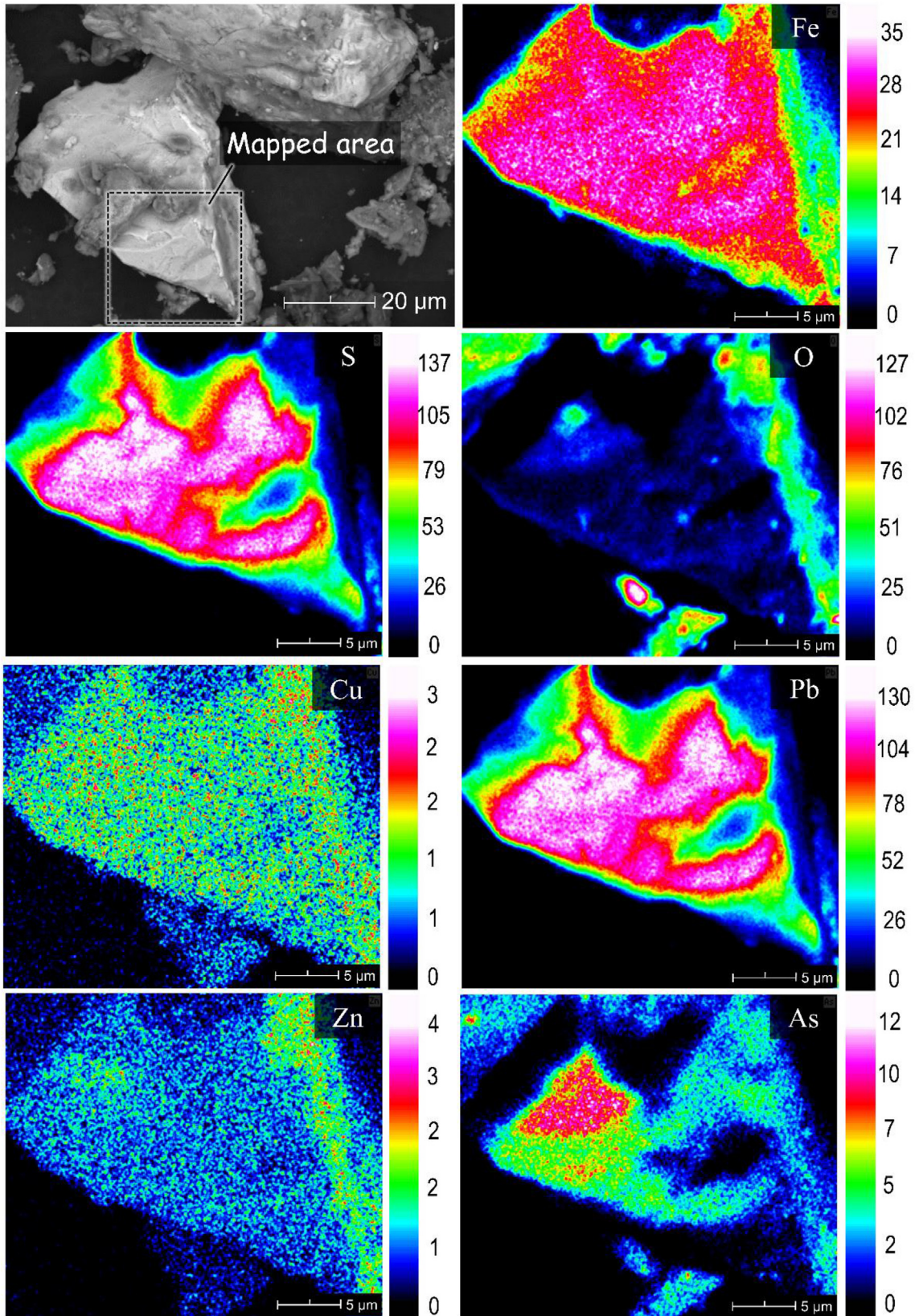
**Fig. 2.** SEM photomicrograph of a representative sulphide mineral in A-1 and the corresponding elemental maps of Fe, S, O, Cu, Pb, Zn and As.
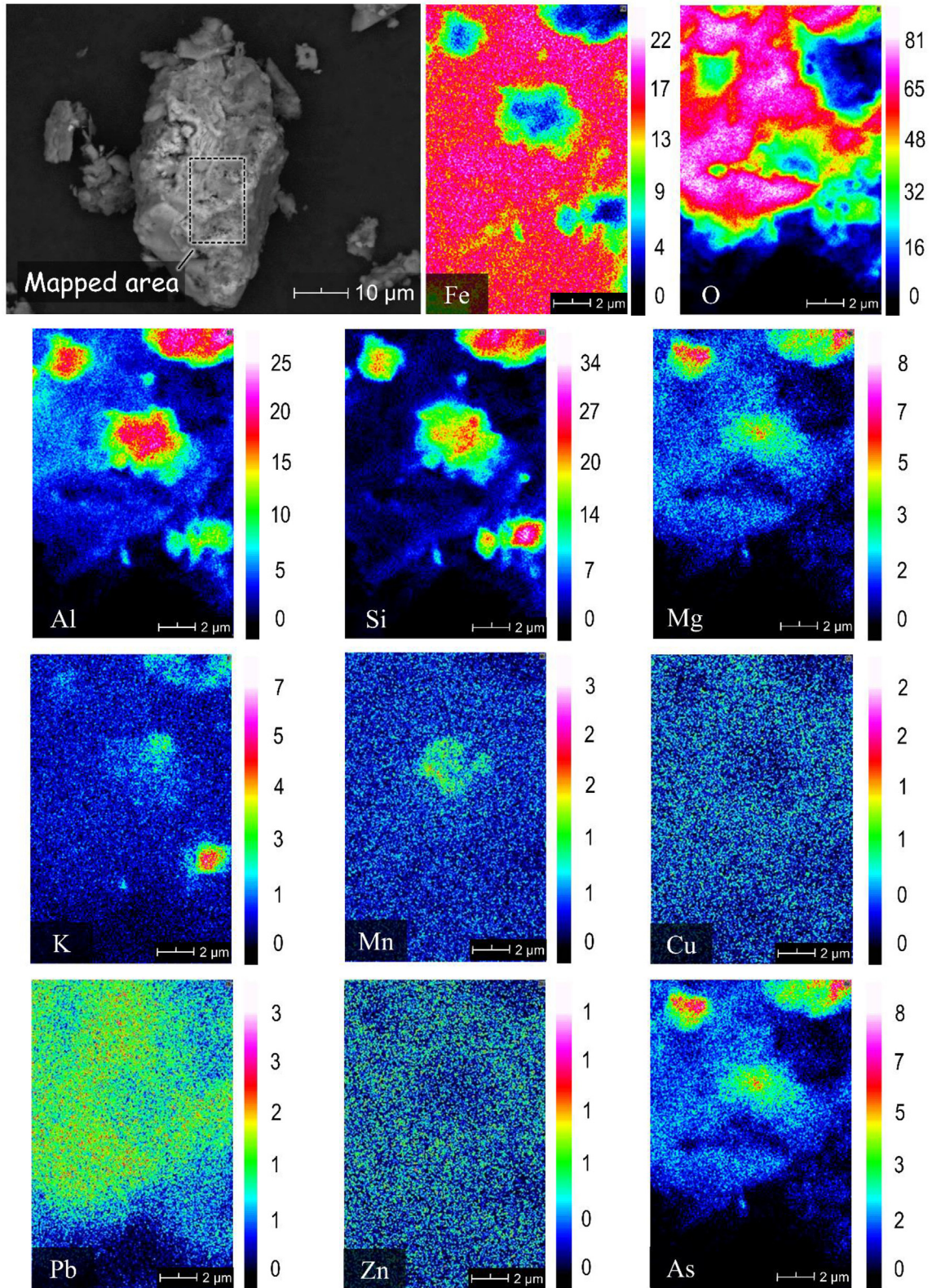
**Fig. 3.** SEM photomicrograph of a representative oxyhydroxide/oxide mineral in A-3 and the corresponding elemental maps of Fe, O, Al, Si, Pb, Mg, K, Mn, Cu, Pb, Zn and As.

A-3 and A-4 to weathering than A-1 and A-2 (Table 2), which likely promoted the dissolution of chalcopyrite and Cu-bearing pyrite (Li et al., 2019b, 2019a; Park et al., 2018; Seng et al., 2019a, 2019b; Tabelin et al., 2017a; Thao et al., 2020), and the subsequent

formations of malachite and goethite (Atapour and Aftabi, 2007; Tabelin and Igarashi, 2009).

Although the bulk of Pb in A-1 and A-2 was associated with reducible (38−39%) and residual (28−50%) phases, those found

**Table 3**
Calculated weathering and pollution indices.

| Sample | CIW | PIA | $I_{geo}$ | | | | CF | | | | CD | PLI |
|---|---|---|---|---|---|---|---|---|---|---|---|---|
| | | | Cu | Pb | Zn | As | Cu | Pb | Zn | As | | |
| A-1 | 23 | 21 | 1 | 6 | 6 | 5 | 4 | 83 | 73 | 68 | 227 | 35 |
| A-2 | 51 | 49 | 0.7 | 4 | 4 | 3 | 3 | 26 | 18 | 14 | 60 | 11 |
| A-3 | 67 | 64 | 0.3 | 3 | 2 | 2 | 2 | 16 | 8 | 5 | 31 | 6 |
| A-4 | 71 | 69 | 0.2 | 3 | 3 | 1 | 2 | 15 | 10 | 4 | 30 | 6 |
| A-5 | 77 | 75 | −0.7 | −0.8 | 0.1 | 0.2 | 1 | 0.9 | 1.6 | 1.7 | 5.1 | 1.2 |
| A-6 | 74 | 72 | −0.6 | −0.6 | −0.3 | 0.2 | 1 | 1 | 1.2 | 1.7 | 4.9 | 1.2 |
| A-7 | 77 | 76 | −0.7 | −0.6 | −1.4 | −2.1 | 0.9 | 1 | 0.6 | 0.3 | 2.8 | 0.6 |
| A-8 | 81 | 80 | −0.4 | −0.4 | −1.2 | −2.7 | 1.2 | 1.1 | 0.6 | 0.2 | 3.2 | 0.7 |

*Note: Operating ASGM site (A-1 and A-2), historic ASGM site (A-3 and A-4) and 'control' sites (A-5 to A-8).

with weak acid soluble (3—16%) and oxidisable (5—10%) fractions were still significant (Fig. 4). Similar to Cu, Pb in the reducible fraction was likely co-precipitated with HFOs (Fig. 4) while those found in the oxidisable phase was mainly partitioned with galena and pyrite (Fig. 3; Supplementary Fig. 2). It is also important to note that Pb in strongly adsorbed fraction of A-1 was around 10%, the bulk of which was likely found with HFOs because of their ability to sequester $Pb^{2+}$ from solution (Sauvé et al., 2000). To a lesser extent, kaolinite and montmorillonite may have also contributed to the strongly adsorbed fraction because $Pb^{2+}$ adsorption to clay minerals is considerable due to their strongly negative surface charge densities (Barbier et al., 2000).

Zinc in the ASGM-impacted soil samples (A-1 to A-4) was predominantly partitioned with three phases—residual (36—45%), reducible (18—36%) and strongly adsorbed (14—28%)—the latter two are considered relatively mobile in the environment. The reducible fraction, mainly composed of HFOs, is readily dissolved under reducing conditions while strongly adsorbed phases are released with changes in soil chemistry like flooding, saltwater intrusion or fertilizer addition (Huyen et al., 2019a; Mar et al., 2013; Nickson et al., 2000; Tabelin and Igarashi, 2009). Similar to Pb, weathering conditions in A-3 and A-4 had dramatic effects on Zn solid-phase partitioning; that is, Zn partitioned with the weak acid soluble phase disappeared while the residual and reducible fractions increased.

The bulk of As in A-1 and A-2 was mainly partitioned with the residual phase (81—95%), but because these two samples were highly contaminated, the amounts found with the strongly adsorbed (~24 mg/kg), reducible (~8 mg/kg), and oxidisable (~0.1 mg/kg) fractions were still significant. In the historic ASGM processing site (A-3 and A-4), As partitioned with the strongly adsorbed and reducible phases dramatically increased (Fig. 5), which could be attributed to As release from sulphide minerals and its subsequent capture by HFOs (Figs. 2 and 3; Supplementary Figs. 3 and 4; Huyen et al., 2019a; Tabelin et al., 2019, 2020). The more abundant phyllosilicates in A-3 and A-4 may have also contributed to the higher As amounts partitioned with the strongly adsorbed phase because although the crystal faces of kaolinite, montmorillonite and Chlinochlore inherently have net negative charges, significant adsorption of As could occur on their crystal 'edges' (Beaulieu and Savage, 2005; Goldberg and Glaubig, 1988).

### 3.4. Leaching of copper, lead, zinc and arsenic and their release-retention mechanisms in the contaminated soil

Fig. 5 illustrates the pH and concentrations of Fe, Cu, Pb, Zn and As after the standard leaching tests, which were compared with the Philippine regulatory standards for Class A and Class C water quality, a classification based on the usage of freshwater in the Philippines. Class A water quality standard is for water bodies used

as drinking water supply after conventional treatment like groundwater and surface waters while Class C water quality standard is for sources of water utilised for irrigation and other agricultural purposes (DENR, 2016). The pH values of leachates from A-1 and A-2 were slightly higher while those in A-7 and A-8 were lower than the Class A environmental standards (pH 6.5—8.5). The slightly alkaline pH of A-1 and A-2 could be attributed to the strong pH-buffering effects of calcite and dolomite (Eang et al., 2018a, b) while the slightly acidic pH in A-7 and A-8 may be related to the impacts of agriculture. Dissolved Fe in the leachate of A-3 exceeded the Class A water quality limit of 1.0 mg/L but passed the 1.5 mg/L environmental standard for Class C effluents. Dissolved Pb and Zn from all samples were below the Class A and Class C water quality standards while leachates from two samples, A-2 and A-3, had dissolved Cu concentrations exceeding the regulatory limits (Fig. 5c—e).

The mobility of heavy metals in contaminated soils, rocks and sediments is typically determined by the balance between release and retention mechanisms under a given geochemical condition (Marove et al., 2020; Silwamba et al., 2020; Tabelin et al., 2018). On one hand, sulphide oxidation is likely the most dominant release mechanism of Cu, Pb and Zn from the ASGM-impacted soils because under oxidising and slightly alkaline (pH 8.2—8.7) conditions, HFOs and carbonates are more stable than sulphide minerals. On the other hand, co-precipitation and adsorption are most likely the two dominant retention mechanisms of these heavy metals in ASGM-impacted soils under these conditions. Retention of dissolved Pb and Zn via adsorption was significant because ASGM-impacted soils contain HFOs, kaolinite and montmorillonite with net negatively charged surfaces between pH 8.2 and 8.7 and could readily sequester positively charged Pb and Zn ions from solution (Abollino et al., 2003; Beaulieu and Savage, 2005; Goldberg and Glaubig, 1988; Veli and Alyüz, 2007).

Noteworthy in the results was the higher Cu concentration in the leachates of historical ASGM-impacted soil samples (A-3 and A-4) compared with those collected from the currently operating ASGM site (A-1 and A-2). To gain additional insights into the reasons why higher Cu leaching was observed in the more weathered soil samples, a geochemical model was created using the React® function of Geochemist's Workbench® (Bethke and Yeakel, 2011). In this model, calcite and dolomite were incrementally added to a solution based on the measured leachate properties of A-3 and A-4. The geochemical model predicts that malachite precipitation and stability are both enhanced with increasing amounts of calcite or dolomite added into the system (Supplementary Fig. 5). Moreover, calcite and dolomite have been reported to sequester $Cu^{2+}$ via adsorption and surface precipitation reactions (Papadopoulos and Rowell, 1989; Parsiegla and Katz, 1999). These results suggest that gradual dissolution of calcite and dolomite in ASGM-impacted soils due to weathering could enhance the mobility of Cu.
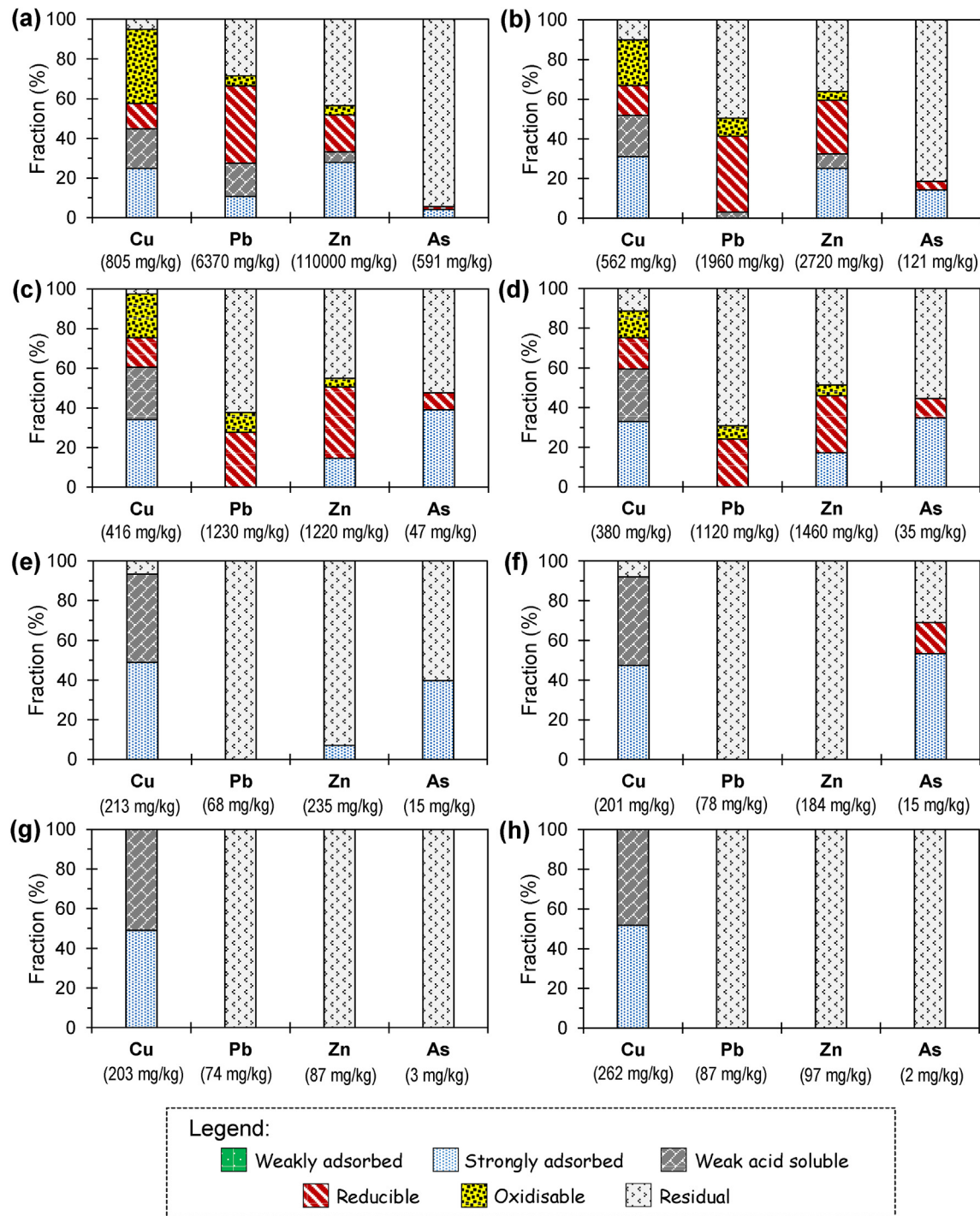
**Fig. 4.** Solid-phase partitioning of Cu, Pb, Zn and As in A-1 (a), A-2 (b), A-3 (c), A-4 (d), A-5 (e), A-6 (f), A-7 (g) and A-8 (h). Note that the Cu, Pb, Zn and As contents of soil samples are also provided in the plots for easy comparison.

The release of As from ASGM-impacted and 'control' soil samples is illustrated in Fig. 5f. The leaching of As in A-3 and A-4 (historic ASGM processing site) both exceeded the Class A and Class C water quality standards while dissolved As in the other soil samples, including A-1 and A-2 (operating ASGM processing site), were negligible. To gain insights into the speciation of dissolved As in the leaching experiments, an equilibrium Eh–pH diagram was created using the Geochemist's Workbench® based on measured concentrations of dissolved solutes, which were converted to solute

activities by PHREEQC (Parkhurst and Apello, 1999). As illustrated in Supplementary Fig. 6, dissolved As under oxidising conditions between pH 6.5 and 11.8 is generally present as the negatively charged $HAsO_4^{2-}$ oxyanion while HFOs, as noted earlier, have negatively charged surfaces above around pH 7.5. This means that at pH ~8.2, As release from A-3 and A-4 was likely promoted by enhanced desorption, a deduction consistent with the significant amounts of As partitioned with strongly adsorbed phase and the reports of other authors (Meng et al., 2002; Wang and Mulligan,
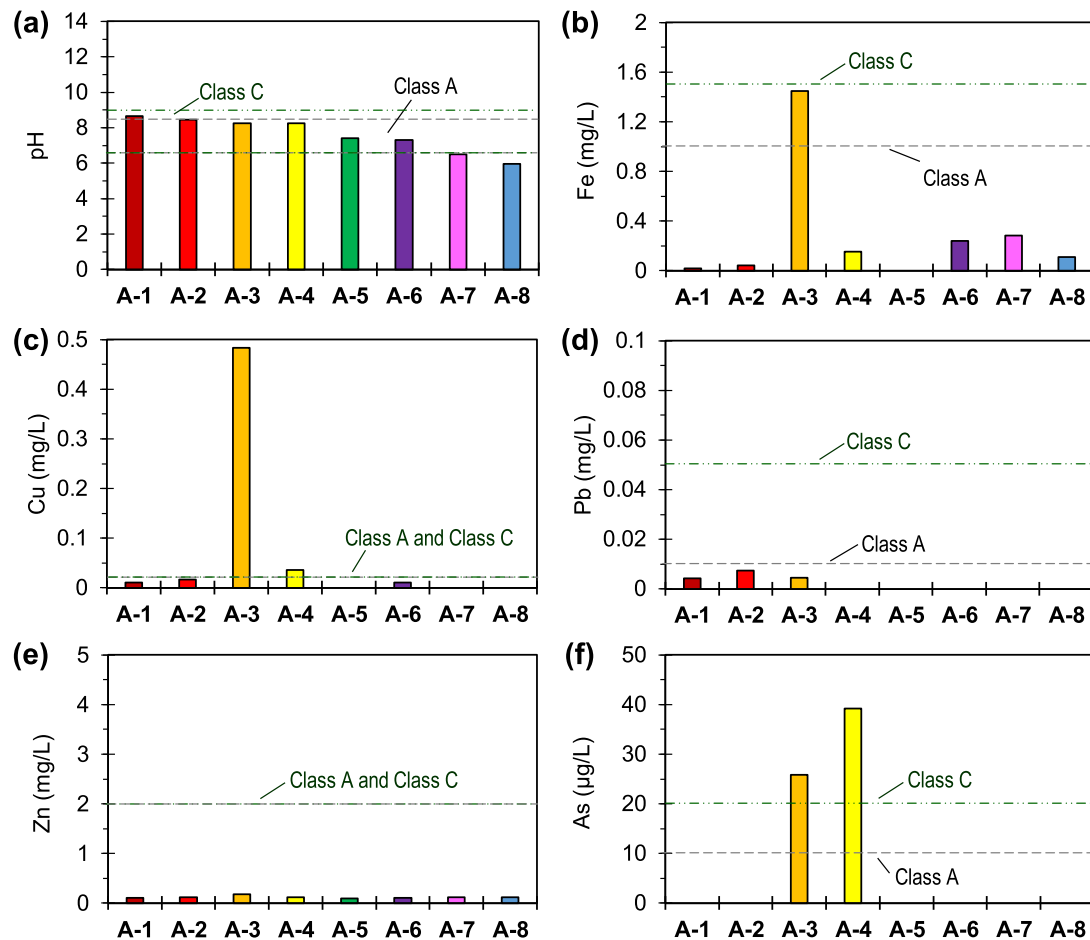
**Fig. 5.** Geochemical properties of leachates after the standard leaching test of 8 soil samples, including the concentrations of major dissolved metals and trace contaminants: pH (a), Fe (b), Cu (c), Pb (d), Zn (e), and As (f). Note that the broken lines in the plots refer to Class A and Class C water quality standards used in the Philippines.

2006). Although A-1 and A-2 also had substantial amounts of As in the strongly adsorbed phase and had similar leachate pH values as those of A-3 and A-4, As mobility was likely limited by the high dolomite contents of these samples. Ayoub and Mehawej (2007), for example, noted the high removal of As from DI water (>92%) and synthetic wastewaters (>84%) using dolomite powder as an adsorbent, a phenomenon later attributed by other authors to the formation Mg–As-carbonate precipitates on the mineral's surface (Salameh et al., 2010).

## 4. Conclusions

This study investigated the solid-phase partitioning of Cu, Pb, Zn and As in ASGM-impacted soils from Davao de Oro, Mindanao, Philippines and identified the major release-retention mechanisms controlling the mobility of these environmentally regulated contaminants. The findings of this work are summarised as follows:

1. Contamination of the soil was mainly attributed to the presence of primary sulphide minerals like pyrite, chalcopyrite, galena and sphalerite accompanying the Au-ores processed on-site.
2. The bulk of Cu, Pb and Zn in the ASGM-impacted soils was partitioned in four phases—strongly adsorbed, weak acid soluble, reducible, and oxidisable—that could become unstable with changes in soil geochemical conditions.

3. Arsenic in the ASGM-impacted soils was mainly associated with strongly adsorbed and reducible fractions, both of which were linked to goethite and HFOs found in the soils.
4. Standard leaching tests showed minimal release of Pb and Zn because of their retention via adsorption-coprecipitation with HFOs and sorption reactions with kaolinite and montmorillonite.
5. The release of Cu and As from historic ASGM-impacted soils exceeded both Class A and Class C water quality standards, which means that ASGM activities without appropriate waste management plans would have deleterious impacts on the surrounding environment and water bodies.

## CRediT authorship contribution statement

**Carlito Baltazar Tabelin:** Conceptualization, Methodology, Investigation, Formal analysis, Writing - original draft. **Marthias Silwamba:** Investigation, Formal analysis, Writing - review & editing. **Florifern C. Paglinawan:** Investigation, Writing - review & editing. **Alissa Jane S. Mondejar:** Investigation, Writing - review & editing. **Ho Gia Duc:** Investigation, Writing - review & editing. **Vannie Joy Resabal:** Investigation, Writing - review & editing. **Einstine M. Opiso:** Investigation, Writing - review & editing. **Toshifumi Igarashi:** Resources, Formal analysis, Writing - review & editing. **Shingo Tomiyama:** Formal analysis, Writing - review &

### Appendix A. Supplementary data

Supplementary data to this article can be found online at https://doi.org/10.1016/j.chemosphere.2020.127574.

### References

Abollino, O., Aceto, M., Malandrino, M., Sarzanini, C., Mentasti, E., 2003. Adsorption of heavy metals on Na-montmorillonite: effect of pH and organic substances. Water Res. 37, 1619—1627.

Abraitis, P.K., Pattrick, R.A.D., Vaughan, D.J., 2004. Variations in the compositional, textural and electrical properties of natural pyrite: a review. Int. J. Miner. Process. 74 (1—4), 41—59.

Adewumi, A.J., Laniyan, T.A., 2020. Contamination, sources and risk assessments of metals in media from Anka artisanal gold mining area, Northwest Nigeria. Sci. Total Environ. 718, 137235.

Anju, M., Banerjee, D.K., 2010. Comparison of two sequential extraction procedures for heavy metal partitioning in mine tailings. Chemosphere 78 (11), 1393—1402.

Aseniero, J.P., Opiso, E.M., Banda, M.H.B., Tabelin, C.B., 2019. Potential utilization of artisanal gold-mine tailings as geopolymeric source material: a preliminary investigation. SN Applied Sciences 1, 35.

Atapour, H., Aftabi, A., 2007. The geochemistry of gossans associated with Sarcheshmeh porphyry copper deposit, Rafsanjan, Kerman, Iran: implications for exploration and the environment. J. Geochem. Explor. 93, 47—65.

Ayoub, G.M., Mehawej, M., 2007. Adsorption of arsenate on untreated dolomite powder. J. Hazard Mater. 148, 259—266.

Babut, M., Sekyi, R., Rambaud, A., Potin-Gautier, M., Tellier, S., Bannerman, W., Beinhoff, C., 2003. Improving the environmental management of small-scale gold mining in Ghana: a case study of Dumasi. J. Clean. Prod. 11, 215—221.

Balan, E., Allard, T., Morin, G., Fritsch, E., Calas, G., 2020. Crystallochemistry of clay minerals, weathering processes and evolution of continental surfaces. In: Electron Paramagnetic Resonance Spectroscopy. Springer, Cham, pp. 109—135.

Barbier, F., Duc, G., Petit-Ramel, M., 2000. Adsorption of lead and cadmium ions from aqueous solution to the montmorillonite/water interface. Colloids Surf. A Physicochem. Eng. Asp. 166, 153—159.

Beaulieu, B.T., Savage, K.S., 2005. Arsenate adsorption structures on aluminum oxide and phyllosilicate mineral surfaces in smelter-impacted soils. Environ. Sci. Technol. 39, 3571—3579.

Bethke, C.M., Yeakel, S., 2011. The Geochemist's Workbench® — a User's Guide to GSS, Rxn, Act2, Tact, Spec8, React, Gtplot, X1t, X2t and Xtplot. Aqueous Solutions LLC, Urbana, Illinois.

Calderon, A.R.M., Alorro, R.D., Tadesse, B., Yoo, K., Tabelin, C.B., 2019. Evaluation of maghemite-rich iron oxide composite prepared from magnetite as adsorbent for gold from chloride solution. J. Occup. Med. 71, 4639—4646.

Calderon, A.R.M., Alorro, R.D., Tadesse, B., Yoo, K., Tabelin, C.B., 2020. Repurposing of nickeliferous pyrrhotite from mine tailings as magnetic adsorbent for the recovery of gold from chloride solution. Resour. Conserv. Recycl. 161, 104971.

Choi, J.R., 2020. Development of point-of-care biosensors for COVID-19. Frontiers in Chemistry 8, 517.

Clevenger, T.E., 1990. Use of sequential extraction to evaluate the heavy metals in mining wastes. Water Air Soil Pollut. 50, 241—253.

Cordy, P., Veiga, M.M., Salih, I., Al-Saadi, S., Console, S., Garcia, O., Mesa, L.A., Velásquez-López, P.C., Roeser, M., 2011. Mercury contamination from artisanal gold mining in Antioquia, Colombia: the world's highest per capita mercury

pollution. Sci. Total Environ. 410, 154—160.

DENR, 2016. Department of Environment and Natural Resources (DENR) Administrative Order No. 2016-08 on Water Quality Guidelines and General Effluent Standards of 2016. https://pab.emb.gov.ph/wp-content/uploads/2017/07/DAO-2016-08-WQG-and-GES.pdf. (Accessed 21 June 2020).

Eang, K.E., Igarashi, T., Fujinaga, R., Kondo, M., Tabelin, C.B., 2018a. Groundwater monitoring of an open-pit limestone quarry: groundwater characteristics, evolution and their connections to rock slopes. Environ. Monit. Assess. 190, 193.

Eang, K.E., Igarashi, T., Kondo, M., Nakatani, T., Tabelin, C.B., Fujinaga, R., 2018b. Groundwater monitoring of an open-pit limestone quarry: water-rock interaction and mixing estimation within the rock layers by geochemical and statistical analyses. International Journal of Mining Science and Technology 28, 849—857.

Ghenciu, A.F., 2002. Review of fuel processing catalysts for hydrogen production in PEM fuel cell systems. Curr. Opin. Solid State Mater. Sci. 6, 389—399.

Ghosh, S., Sullivan, C.A.W., Zerkowski, M.P., Molinaro, A.M., Rimm, D.L., Camp, R.L., Chung, G.G., 2008. High levels of vascular endothelial growth factor and its receptors (VEGFR-1, VEGFR-2, neuropilin-1) are associated with worse outcome in breast cancer. Hum. Pathol. 39, 1835—1843.

Goldberg, S., Glaubig, R.A., 1988. Anion sorption on a calcareous, montmorillonitic soil-selenium. Soil Sci. Soc. Am. J. 52, 954—958.

Grosell, M., Blanchard, J., Brix, K.V., Gerdes, R., 2007. Physiology is pivotal for interactions between salinity and acute copper toxicity to fish and invertebrates. Aquat. Toxicol. 84, 162—172.

Hewitt, A., 2019. ASM Mine Production — Bigger than We Thought. https://www.gold.org/goldhub/gold-focus/2019/05/asm-mine-production-bigger-we-thought. (Accessed 17 June 2020).

Hua, M., Zhang, S., Pan, B., Zhang, W., Lu, L., Zhang, Q., 2012. Heavy metal removal from water/wastewater by nanosized metal oxides: a review. J. Hazard Mater. 211, 317—331.

Huang, D., Kilic, M., 2019. Gold, platinum, and expected stock returns. J. Financ. Econ. 132, 50—75.

Hughes, M.F., 2002. Arsenic toxicity and potential mechanisms of action. Toxicol. Lett. 133, 1—16.

Huston, D.L., Sie, S.H., Sauter, G.F., Cook, D.R., Both, R.A., 1995. Trace elements in sulfide minerals from eastern Australian volcanic-hosted massive sulfide deposits: part 1. Proton microprobe analyses of pyrite, chalcopyrite, and sphalerite, and part 2. Selenium levels in pyrite: comparison with $\delta^{34}S$ values and implications for the source of sulfur in volcanogenic hydrothermal systems. Econ. Geol. 90, 1167—1196.

Huyen, D.T., Tabelin, C.B., Thuan, H.M., Dang, D.H., Truong, P.T., Vongphuthone, B., Kobayashi, M., Igarashi, T., 2019a. The solid-phase partitioning of arsenic in unconsolidated sediments of the Mekong Delta, Vietnam and its modes of release under various conditions. Chemosphere 233, 512—523.

Huyen, D.T., Tabelin, C.B., Thuan, H.M., Danga, D.H., Truong, P.T., Vongphuthone, B., Kobayashi, M., Igarashi, T., 2019b. Geological and Geochemical Characterizations of Sediments in Six Borehole Cores from the Arsenic-Contaminated Aquifer of the Mekong Delta. Vietnam. Data in Brief, p. 104230.

Igarashi, T., Herrera, S.P., Uchiyama, H., Miyamae, H., Iyatomi, N., Hashimoto, K., Tabelin, C.B., 2020. The two-step neutralization ferrite-formation process for sustainable acid mine drainage treatment: removal of copper, zinc and arsenic, and the influence of coexisting ions on ferritization. Sci. Total Environ. 715, 136877.

Jeon, S., Ito, M., Tabelin, C.B., Pongsumrankul, R., Kitajima, N., Park, I., Hiroyoshi, N., 2018a. Gold recovery from shredder light fraction of E-waste recycling plant by flotation-ammonium thiosulfate leaching. Waste Manag. 77, 195—202.

Jeon, S., Tabelin, C.B., Takahashi, H., Park, I., Ito, M., Hiroyoshi, N., 2018b. Interference of coexisting copper and aluminum on the ammonium thiosulfate leaching of gold from printed circuit boards of waste mobile phones. Waste Manag. 81, 148—156.

Jeon, S., Ito, M., Tabelin, C.B., Pongsumrankul, R., Tanaka, S., Kitajima, N., Saito, A., Park, I., Hiroyoshi, N., 2019. A physical separation scheme to improve ammonium thiosulfate leaching of gold by separation of base metals in crushed mobile phones. Miner. Eng. 138, 168—177.

Jeon, S., Tabelin, C.B., Park, I., Nagata, Y., Ito, M., Hiroyoshi, N., 2020a. Ammonium thiosulfate extraction of gold from printed circuit boards (PCBs) of end-of-life mobile phones and its recovery from pregnant leach solution by cementation. Hydrometallurgy 191, 105214.

Jeon, S., Tabelin, C.B., Takahashi, H., Park, I., Ito, M., Hiroyoshi, N., 2020b. Enhanced cementation of gold via galvanic interactions using activated carbon and zero-valent aluminum: A novel approach to recover gold ions from ammonium thiosulfate medium. Hydrometallurgy 191, 105165.

JLT-13, 1973. Departmental Notification No. 13 on Leaching Test Method for Landfill Wastes. Japanese Environmental Agency.

Li, X., Hiroyoshi, N., Tabelin, C.B., Naruwa, K., Harada, C., Ito, M., 2019a. Suppressive effects of ferric-catecholate complexes on pyrite oxidation. Chemosphere 214, 70—78.

Li, X., Gao, M., Hiroyoshi, N., Tabelin, C.B., Taketsugu, T., Ito, M., 2019b. Suppression of pyrite oxidation by ferric-catecholate complexes: An electrochemical study. Miner. Eng. 138, 226—237.

Löfås, S., Johnsson, B., 1990. A novel hydrogel matrix on gold surfaces in surface plasmon resonance sensors for fast and efficient covalent immobilization of ligands. J. Chem. Soc., Chem. Commun. 21, 1526—1528.

Lucarelli, F., Marrazza, G., Turner, A.P., Mascini, M., 2004. Carbon and gold electrodes as electrochemical transducers for DNA hybridisation sensors. Biosens.

Bioelectron. 19, 515—530.

Male, Y.T., Reichelt-Brushett, A.J., Pocock, M., Nanlohy, A., 2013. Recent mercury contamination from artisanal gold mining on Buru Island, Indonesia—Potential future risks to environmental health and food safety. Mar. Pollut. Bull. 77, 428—433.

Mar, K.K., Karnawati, D., Putra, D.P.E., Igarashi, T., Tabelin, C.B., 2013. Comparison of arsenic adsorption on lignite, bentonite, shale, and iron sand from Indonesia. Procedia Earth and Planetary Science 6, 242—250.

Marove, C.A., Tangviroon, P., Tabelin, C.B., Igarashi, T., 2020. Leaching of hazardous elements from Mozambican coal and coal ash. J. Afr. Earth Sci. 168, 103861.

Marshall, B.G., Veiga, M.M., da Silva, H.A., Guimarães, J.R.D., 2020. Cyanide Contamination of the Puyango-Tumbes River Caused by Artisanal Gold Mining in Portovelo-Zaruma, EcuadorCurr Envir Health Rpt. https://doi.org/10.1007/s40572-020-00276-3.

Marumo, K., Ebashi, T., Ujiie, T., 2003. Heavy metal concentrations, leachabilities and lead isotope ratios of Japanese soils. Shigen Chishitsu 53, 125—146 (Paper in Japanese with English abstract).

McLennan, S.M., Hemming, S., McDaniel, D.K., Hanson, G.N., 1993. Geochemical approaches to sedimentation, provenance and tectonics. In: Johnsson, M.J., Basu, A. (Eds.), Processes Controlling the Composition of Clastic Sediments. 285. Geological Society of America, pp. 21—40.

Meng, X., Korfiatis, G.P., Bang, S., Bang, K.W., 2002. Combined effects of anions on arsenic removal by iron hydroxides. Toxicol. Lett. 133, 103—111.

Mol, J.H., Ramlal, J.S., Lietar, C., Verloo, M., 2001. Mercury contamination in freshwater, estuarine, and marine fishes in relation to small-scale gold mining in Suriname, South America. Environ. Res. 86, 183—197.

Nazari, A.M., Radzinski, R., Ghahreman, A., 2017. Review of arsenic metallurgy: treatment of arsenical minerals and the immobilization of arsenic. Hydrometallurgy 174, 258—281.

Needleman, H., 2004. Lead poisoning. Annu. Rev. Med. 55, 209—222.

Nickson, R.T., McArthur, K.M., Ravenscroft, J.M., Burgess, W.G., Ahmed, K.M., 2000. Mechanism of arsenic release to groundwater, Bangladesh, and West Bengal. Appl. Geochem. 15, 403—413.

Opiso, E.M., Aseniero, J.P., Banda, M.T., Tabelin, C.B., 2018. Solid-phase partitioning of mercury in artisanal gold mine tailings from selected key areas in Mindanao, Philippines, and its implications for mercury detoxification. Waste Manag. Res. 36, 269—276.

Paciotti, G.F., Myer, L., Weinreich, D., Goia, D., Pavel, N., McLaughlin, R.E., Tamarkin, L., 2004. Colloidal gold: a novel nanoparticle vector for tumor directed drug delivery. Drug Deliv. 11, 169—183.

Papadopoulos, P., Rowell, D.L., 1989. The reactions of copper and zinc with calcium carbonate surfaces. J. Soil Sci. 40 (1), 39—48.

Park, I., Tabelin, C.B., Seno, K., Jeon, S., Ito, M., Hiroyoshi, N., 2018. Simultaneous suppression of acid mine drainage formation and arsenic release by carrier-microencapsulation using aluminum-catecholate complexes. Chemosphere 205, 414—425.

Park, I., Tabelin, C.B., Jeon, S., Li, X., Seno, K., Ito, M., Hiroyoshi, N., 2019. A review of recent strategies for acid mine drainage prevention and mine tailings recycling. Chemosphere 219, 588—606.

Parkhurst, D.L., Appelo, C.A.J., 1999. User's guide to PHREEQC (version 2) — a computer program for speciation, batch-reactions, one-dimensional transport, and inverse geochemical calculations. U.S. Department of the Interior and U.S. Geological Survey. Water Resour. Invest. Rep. 99—4259.

Parsiegla, K.I., Katz, J.L., 1999. Calcite growth inhibition by copper (II): I. Effect of supersaturation. J. Cryst. Growth 200 (1—2), 213—226.

Phengsaart, T., Ito, M., Hamaya, N., Tabelin, C.B., Hiroyoshi, N., 2018. Improvement of jig efficiency by shape separation, and a novel method to estimate the separation efficiency of metal wires in crushed electronic wastes using bending behavior and "entanglement factor". Miner. Eng. 129, 54—62.

Phengsaart, T., Ito, M., Azuma, A., Tabelin, C.B., Hiroyoshi, N., 2020. Jig separation of crushed plastics: the effects of particle geometry on separation efficiency. J. Mater. Cycles Waste Manag. 22, 787—800.

Philippine Statistics Authority (Psa), 2017. Estimation of Production, Tons Mined and Tailing Generated by the Small-Scale Gold Mining Activities. https://psa.gov.ph/content/estimation-production-tons-mined-and-tailing-generated-small-scale-gold-mining-activities. (Accessed 29 February 2020).

Pirajno, F., 2009. Hydrothermal Processes and Mineral Systems. Springer Science, The Netherlands.

Portnoy, M.E., Rosenzweig, A.C., Rae, T., Huffman, D.L., O'Halloran, T.V., Culotta, V.C., 1999. Structure-function analyses of the ATX1 metallochaperone. J. Biol. Chem. 274, 15041—15045.

Salameh, Y., Al-Lagtah, N., Ahmad, M.N.M., Allen, S.J., Walker, G.M., 2010. Kinetic and thermodynamic investigations on arsenic adsorption onto dolomitic sorbents. Chem. Eng. J. 160, 440—446.

Salgueiro, M.J., Zubillaga, M., Lysionek, A., Sarabia, M.I., Caro, R., Paoli, T.D., Hager, A., Weill, R., Boccio, J., 2000. Zinc as an essential micronutrient: a review. Nutr. Res. 20, 737—755.

Sauvé, S., Martí nez, C.E., McBride, M., Hendershot, W., 2000. Adsorption of free lead (Pb2+) by pedogenic oxides, ferrihydrite, and leaf compost. Soil Sci. Soc. Am. J. 64 (2), 595—599.

Seng, S., Tabelin, C.B., Kojima, M., Hiroyoshi, N., Ito, M., 2019a. Galvanic microencapsulation (GME) using zero-valent aluminum and zero-valent iron to suppress pyrite oxidation. Mater. Trans. 60 (2), 277—286.

Seng, S., Tabelin, C.B., Makino, Y., Chea, M., Phengsaart, T., Park, I., Hiroyoshi, N., Ito, M., 2019b. Improvement of flotation and suppression of pyrite oxidation

using phosphate-enhanced galvanic microencapsulation (GME) in a ball mill with steel ball media. Miner. Eng. 143, 105931.

Silwamba, M., Ito, M., Hiroyoshi, N., Tabelin, C.B., Fukushima, T., Park, I., Jeon, S., Igarashi, T., Sato, T., Nyambe, I., Chirwa, M., Banda, K., Nakata, H., Nakayama, S., Ishizuka, M., 2020. Detoxification of lead-bearing zinc plant leach residues from Kabwe, Zambia by coupled extraction-cementation method. Journal of Environmental Chemical Engineering 104197. https://doi.org/10.1016/j.jece.2020.104197.

Silwamba, M., Ito, M., Hiroyoshi, N., Tabelin, C.B., Hashizume, R., Fukushima, T., Park, I., Jeon, S., Igarashi, T., Sato, T., Chirwa, M., Banda, K., Nyambe, I., Nakata, H., Nakayama, S., Ishizuka, M., 2020. Recovery of lead and zinc from zinc plant leach Residues by concurrent dissolution-cementation using zero-valent aluminum in chloride medium. Metals 10 (4), 531.

Singer, D.A., Berger, V.I., Moring, B.C., 2008. Porphyry Copper Deposits of the World: Database and Grade and Tonnage Models: USGS Open-File Report 2008-1155.

Smedley, P.L., Kinniburgh, D.G., 2002. A review of the source, behavior, and distribution of arsenic in natural waters. Appl. Geochem. 17, 517—568.

Steckling, N., Boese-O'Reilly, S., Gradel, C., Gutschmidt, K., Shinee, E., Altangerel, E., Badrakh, B., Bonduush, I., Surenjav, U., Ferstl, P., Roider, G., 2011. Mercury exposure in female artisanal small-scale gold miners (ASGM) in Mongolia: an analysis of human biomonitoring (HBM) data from 2008. Sci. Total Environ. 409, 994—1000.

Swain, E.B., Jakus, P.M., Rice, G., Lupi, F., Maxson, P.A., Pacyna, J.M., Penn, A., Spiegel, S.J., Veiga, M.M., 2007. Socioeconomic consequences of mercury use and pollution. Ambio 45—61.

Tabelin, C.B., Igarashi, T., 2009. Mechanisms of arsenic and lead release from hydrothermally altered rock. J. Hazard Mater. 169, 980—990.

Tabelin, C.B., Igarashi, T., Tamoto, S., 2010. Factors affecting arsenic mobility from hydrothermally altered rock in impoundment-type in situ experiments. Miner. Eng. 23, 238—248.

Tabelin, C.B., Igarashi, T., Tamoto, S., Takahashi, R., 2012a. The roles of pyrite and calcite in the mobilization of arsenic and lead from hydrothermally altered rocks excavated in Hokkaido, Japan. J. Geochem. Explor. 119—120, 17—31.

Tabelin, C.B., Igarashi, T., Takahashi, R., 2012b. Mobilization and speciation of arsenic from hydrothermally altered rock in laboratory column experiments under ambient conditions. Appl. Geochem. 27, 326—342.

Tabelin, C.B., Igarashi, T., Yoneda, T., Tamamura, S., 2013. Utilization of natural and artificial adsorbents in the mitigation of arsenic leached from hydrothermally altered rock. Eng. Geol. 156, 58—67.

Tabelin, C.B., Hashimoto, A., Igarashi, T., Yoneda, T., 2014a. Leaching of boron, arsenic, and selenium from sedimentary rocks: II. pH dependence, speciation, and mechanisms of release. Sci. Total Environ. 473—474, 244—253.

Tabelin, C.B., Hashimoto, A., Igarashi, T., Yoneda, T., 2014b. Leaching of boron, arsenic and selenium from sedimentary rocks: I. Effects of contact time, mixing speed and liquid-to-solid ratio. Sci. Total Environ. 472, 620—629.

Tabelin, C.B., Igarashi, T., Arima, T., Sato, D., Tatsuhara, T., Tamoto, S., 2014c. Characterization and evaluation of arsenic and boron adsorption onto natural geologic materials, and their application in the disposal of excavated altered rock. Geoderma 213, 163—172.

Tabelin, C.B., Veerawattananun, S., Ito, M., Hiroyoshi, N., Igarashi, T., 2017a. Pyrite oxidation in the presence of hematite and alumina: II. Effects on the cathodic and anodic half-cell reactions. Sci. Total Environ. 581—582, 126—135.

Tabelin, C.B., Sasaki, R., Igarashi, T., Park, I., Tamoto, S., Arima, T., Ito, M., Hiroyoshi, N., 2017b. Simultaneous leaching of arsenite, arsenate, selenite, and selenate, and their migration in tunnel-excavated sedimentary rocks: I. Column experiments under intermittent and unsaturated flow. Chemosphere 186, 558—569.

Tabelin, C.B., Sasaki, R., Igarashi, T., Park, I., Tamoto, S., Arima, T., Ito, M., Hiroyoshi, N., 2017c. Simultaneous leaching of arsenite, arsenate, selenite, and selenate, and their migration in tunnel-excavated sedimentary rocks: II. Kinetic and reactive transport modeling. Chemosphere 188, 444—454.

Tabelin, C.B., Igarashi, T., Villacorte-Tabelin, M., Park, I., Opiso, E.M., Ito, M., Hiroyoshi, N., 2018. Arsenic, selenium, boron, lead, cadmium, copper, and zinc in naturally contaminated rocks: a review of their sources, modes of enrichment, mechanisms of release, and mitigation strategies. Sci. Total Environ. 645, 1522—1553.

Tabelin, C.B., Corpuz, R.D., Igarashi, T., Villacorte-Tabelin, M., Ito, M., Hiroyoshi, N., 2019. Hematite-catalysed scorodite formation as a novel arsenic immobilisation strategy under ambient conditions. Chemosphere 233, 946—953.

Tabelin, C.B., Corpuz, R.D., Igarashi, T., Villacorte-Tabelin, M., Alorro, R.D., Yoo, K., Raval, S., Ito, M., Hiroyoshi, N., 2020. Acid mine drainage formation and arsenic mobility under strongly acidic conditions: importance of soluble phases, iron oxyhydroxides/oxides and nature of oxidation layer on pyrite. J. Hazard Mater. 399, 122844.

Tack, F.M.G., Verloo, M.G., 1995. Chemical speciation and fractionation in soil and sediment heavy metal analysis: a review. Int. J. Environ. Anal. Chem. 59, 225—238.

Tamoto, S., Tabelin, C.B., Igarashi, T., Ito, M., d Hiroyoshi, N., 2015. Short and long term release mechanisms of arsenic, selenium and boron from a tunnel-excavated sedimentary rock under in situ conditions. J. Contam. Hydrol. 175, 60—71.

Tatsuhara, T., Arima, T., Igarashi, T., Tabelin, C.B., 2012. Combined neutralization—adsorption system for the disposal of hydrothermally altered excavated rock producing acidic leachate with hazardous elements. Eng. Geol. 139, 76—84.

Tessier, A., Campbell, G.C., Bisson, M., 1979. Sequential extraction procedure for the speciation of particulate trace metals. Anal. Chem. 51, 844–850.

Thao, N.T.P., Tsuji, S., Jeon, S., Park, I., Tabelin, C.B., Ito, M., Hiroyoshi, N., 2020. Redox potential-dependent chalcopyrite leaching in acidic ferric chloride solutions: leaching experiments. Hydrometallurgy. https://doi.org/10.1016/j.hydromet.2020.105299.

Tomiyama, S., Igarashi, T., Tabelin, C.B., Tangviroon, P., Ii, H., 2019. Acid mine drainage sources and hydrogeochemistry at the Yatani mine, Yamagata, Japan: a geochemical and isotopic study. J. Contam. Hydrol. 225, 103502.

Tomiyama, S., Igarashi, T., Tabelin, C.B., Tangviroon, P., Ii, H., 2020. Modeling of the groundwater flow system in excavated areas of an abandoned mine. J. Contam. Hydrol. 230, 103617.

Van Straaten, P., 2000. Mercury contamination associated with small-scale gold mining in Tanzania and Zimbabwe. Sci. Total Environ. 259, 105–113.

Veiga, M.M., Hinton, J.J., 2002. February. Abandoned artisanal gold mines in the Brazilian Amazon: a legacy of mercury pollution. In: Natural Resources Forum, vol. 26. Blackwell Publishing Ltd, Oxford, UK and Boston, USA, pp. 15–26. No. 1.

Veiga, M.M., Schorscher, J.H.D., Fyfe, W.S., 1991. Relationship of copper with hydrous ferric oxides: salobo, carajas, para, Brazil. Ore Geol. Rev. 6, 245–255.

Veiga, M.M., Angeloci-Santos, G., Meech, J.A., 2014. Review of barriers to reduce mercury use in artisanal gold mining. The Extractive Industries and Society 1, 351–361.

Velásquez-López, P.C., Veiga, M.M., Klein, B., 2011. Cyanidation of mercury-rich tailings in artisanal and small-scale mining: identifying strategies to manage environmental risks in Southern Ecuador. J. Clean. Prod. 19, 1125–1133.

Veli, S., Alyüz, B., 2007. Adsorption of copper and zinc from aqueous solutions by using natural clay. J. Hazard Mater. 149, 226–233.

Verbrugge, B., 2015. The economic logic of persistent informality: artisanal and small-scale mining in the southern Philippines. Dev. Change 46, 1023–1046.

Verbrugge, B., 2020. The Philippines: state-sanctioned informalization. In: Global Gold Production Touching Ground. Palgrave Macmillan, Cham, pp. 339–355.

Violante, A., Ricciardella, M., Pigna, M., 2003. Adsorption of heavy metals on mixed Fe-Al oxides in the absence or presence of organic ligands. Water Air Soil Pollut. 145, 289–306.

Wang, S., Mulligan, C.N., 2006. Natural attenuation processes for remediation of arsenic contaminated soils and groundwater. J. Hazard Mater. 138, 459–470.

World Gold Council, 2020a. Gold Supply and Demand Statistics. https://www.gold.org/goldhub/data/gold-supply-and-demand-statistics. (Accessed 17 June 2020).

World Gold Council, 2020b. Gold Prices. https://www.gold.org/goldhub/data/gold-prices. (Accessed 17 June 2020).

Zielasek, V., Jürgens, B., Schulz, C., Biener, J., Biener, M.M., Hamza, A.V., Bäumer, M., 2006. Gold catalysts: nanoporous gold foams. Angew. Chem. Int. Ed. 45, 8241–8244.